



Highlighting research results from the Center for Nanophase Materials Sciences at Oak Ridge National Laboratory. This representative watercolor illustration was painted by Sallie Wolf.

Title: Dynamic morphologies of microscale droplet interface bilayers

This work characterizes the dynamic behavior of droplet interface bilayers, such as buckling and fission, that spontaneously occur as the droplets shrink due to evaporation.

As featured in:



See C. Patrick Collier et al.,  
*Soft Matter*, 2014, 10, 2530.



[www.softmatter.org](http://www.softmatter.org)

Registered charity number: 207890

# Dynamic morphologies of microscale droplet interface bilayers†

 Cite this: *Soft Matter*, 2014, 10, 2530

 Prachya Mruetusatorn,<sup>a</sup> Jonathan B. Boreyko,<sup>b</sup> Guru A. Venkatesan,<sup>c</sup>  
 Stephen A. Sarles,<sup>c</sup> Douglas G. Hayes<sup>a</sup> and C. Patrick Collier<sup>\*b</sup>

Droplet interface bilayers (DIBs) are a powerful platform for studying the dynamics of synthetic cellular membranes; however, very little has been done to exploit the unique dynamical features of DIBs. Here, we generate microscale droplet interface bilayers ( $\mu$ DIBs) by bringing together femtoliter-volume water droplets in a microfluidic oil channel, and characterize morphological changes of the  $\mu$ DIBs as the droplets shrink due to evaporation. By varying the initial conditions of the system, we identify three distinct classes of dynamic morphology. (1) Buckling and fission: when forming  $\mu$ DIBs using the lipid-out method (lipids in oil phase), lipids in the shrinking monolayers continually pair together and slide into the bilayer to conserve their mass. As the bilayer continues to grow, it becomes confined, buckles, and eventually fissions one or more vesicles. (2) Uniform shrinking: when using the lipid-in method (lipids in water phase) to form  $\mu$ DIBs, lipids uniformly transfer from the monolayers and bilayer into vesicles contained inside the water droplets. (3) Stretching and unzipping: finally, when the droplets are pinned to the wall(s) of the microfluidic channel, the droplets become stretched during evaporation, culminating in the unzipping of the bilayer and droplet separation. These findings offer a better understanding of the dynamics of coupled lipid interfaces.

Received 4th December 2013

Accepted 5th February 2014

DOI: 10.1039/c3sm53032a

[www.rsc.org/softmatter](http://www.rsc.org/softmatter)

## 1. Introduction

All biological membranes are composed of lipid bilayers as a fundamental structural element with two opposing layers of amphipathic lipid molecules. Cellular and intracellular membranes in nature are dynamic systems, exhibiting continual shape-change and even experiencing fusion and fission during endo- and exocytosis.<sup>1</sup> To better characterize the dynamics of cellular membranes, synthetic lipid bilayers have been fabricated in the form of vesicles<sup>2</sup> or planar bilayers.<sup>3,4</sup> Synthetic lipid vesicles exhibited budding, fusion, and fission when subjected to osmotic pressure,<sup>5–7</sup> interactions with biomolecules,<sup>8–12</sup> or wetting with interior aqueous compartments.<sup>13–15</sup> The morphology change of supported planar bilayers was investigated by straining the supporting interface<sup>16,17</sup> or by introducing additional biomolecules.<sup>18–20</sup> Suspended planar membranes formed across an aperture opened in a solid wall were perturbed by an impinging fluid jet to fission giant vesicles.<sup>21</sup>

In recent years, droplet interface bilayers (DIBs)<sup>22</sup> have shown great potential as model membranes due to desirable features including stability,<sup>23–27</sup> ease of electrical characterization,<sup>28–30</sup> and the option to form asymmetric bilayers using the lipid-in method.<sup>23</sup> DIBs can be formed by joining together two or more aqueous droplets encapsulated with lipid monolayers in an oil bath; the lipids can either be introduced in the oil phase (lipid-out)<sup>22</sup> or inside the droplets (lipid-in).<sup>23</sup> Most DIBs have been assembled by manually connecting millimetric aqueous droplets using a pipette,<sup>22,29–32</sup> electrodes,<sup>23–27,33–37</sup> or lasers.<sup>38,39</sup> Alternatively, a single aqueous volume can be divided into multiple compartments and then attached together using a flexible substrate.<sup>28,40</sup> Microfluidic DIBs have also been fabricated using dielectrophoresis,<sup>41</sup> electrowetting on dielectric (EWOD),<sup>42,43</sup> thin tubes,<sup>44,45</sup> flow focusing,<sup>46</sup> or 3D printing.<sup>47</sup> Recently, it has become apparent that DIBs offer distinct advantages for dynamic membrane characterization. For regular suspended membranes (formed in apertures), the aperture size is fixed, preventing the membrane from changing its size, while the area and thickness of DIBs can be tuned by controlling the size and curvature of the droplets.<sup>26</sup> Another novel aspect of DIBs is the interplay between the bilayer and the connecting monolayers, which is not present in other model systems.<sup>48</sup> However, most studies to date have only focused on steady-state DIBs and very little has been done to exploit their unique dynamical features.

In our previous work, we passively induced dramatic shape changes into microscale DIBs *via* droplet evaporation to examine how the monolayer–bilayer coupling affected the

<sup>a</sup>Department of Biosystems Engineering & Soil Science, The University of Tennessee, Knoxville, Tennessee 37996, USA

<sup>b</sup>Center for Nanophase Materials Sciences, Oak Ridge National Laboratory, Oak Ridge, Tennessee 37831, USA. E-mail: [colliercp@ornl.gov](mailto:colliercp@ornl.gov)

<sup>c</sup>Department of Mechanical, Aerospace and Biomedical Engineering, The University of Tennessee, Knoxville, Tennessee 37996, USA

† Electronic supplementary information (ESI) available: Four supplemental figures (Fig. S1–S4) and 13 movies of evaporating  $\mu$ DIBs. See DOI: 10.1039/c3sm53032a

membrane dynamics.<sup>48</sup> During evaporation, lipids in the shrinking monolayers were forced to slide into the growing bilayer, causing the bilayer to become confined, buckle, and ultimately fission vesicles to mitigate its stress. This transfer of lipids between multiple interfaces could shed light on lipid interactions that naturally occur between vesicles and membranes during endo- and exocytosis. The transfer of lipids between various membranes is also of importance in engineered systems. For example, supported lipid bilayers are fabricated by transferring lipids from vesicles to a substrate; the kinetics of such processes is only beginning to be understood.<sup>49–54</sup> The rate of lipid diffusion to an interface with a non-equilibrium lipid concentration was found to be dependent on the curvature of the interface<sup>55</sup> and on the length scale and flow field of the fluidic system.<sup>56</sup> Much remains to be understood regarding lipid transfer between membranes, particularly for the case of DIBs where multiple lipid interfaces are coupled together.

Here, we form microscale droplet interface bilayers ( $\mu$ DIBs) in a microfluidic channel to characterize the dynamic morphologies of the coupled monolayers and bilayer membranes during evaporation. Using both the lipid-in and lipid-out techniques to create  $\mu$ DIBs from femtoliter-volume droplets, we identify three distinct classes of lipid transfer during evaporation that are dependent upon the initial conditions of the system. (1) Buckling and fission: when the lipids are well dissolved in the continuous oil phase, the energetic favorability of the formed bilayer coupled with droplet evaporation causes a “conveyor-belt” effect, where lipids in the shrinking monolayer interfaces pair together and slide into the growing bilayer interface to conserve their mass. As the shrinking monolayers continue to grow into the bilayer, the bilayer becomes confined, buckles, and eventually fissions a satellite vesicle. While this behavior was characterized in a recent communication for a two droplet system,<sup>48</sup> here we induce directional buckling and fission for droplets of different sizes and observe multiple buckling events for droplet networks composed of several  $\mu$ DIBs. (2) Uniform shrinking: when the lipid-in approach is used to generate vesicles inside of the water droplets, lipids favor transferring from both the monolayers and the bilayer into the inner vesicles. This lipid transfer occurs at a fairly even rate, resulting in the uniform shrinkage of the droplets with no net change in shape. (3) Stretching and unzipping: when at least one of the droplets is pinned to a wall of the microfluidic device, the droplets become stretched during evaporation. This eventually pulls apart the bilayer, resulting in the complete detachment and separation of the droplets. Interestingly, a unique form of lipid dynamics was observed for pinned droplets: lipids transferred from the shrinking droplets to satellite droplets that nucleated and grew about the parent droplet's interface. To our knowledge, classes (2) and (3) of lipid transfer are novel and have not been previously reported. These findings can lead to a better understanding of the dynamic morphology of coupled lipid interfaces.

## 2. Experimental

### 2.1. Fabrication of microfluidic devices

Poly(dimethylsiloxane) (PDMS) was patterned and bonded to PDMS-coated glass cover slips to construct microfluidic devices.

Two opposing side-channels ( $1\ \mu\text{m} \times 1\ \mu\text{m}$ ) were connected to either side of a larger central channel ( $14.6\ \mu\text{m}$  wide  $\times$   $18\ \mu\text{m}$  high). The fabrication methodology was described in detail in previous papers.<sup>57,58</sup>

### 2.2. Preparation of lipid–oil mixtures

The oils employed here included purified soybean oil and hexadecane (Sigma-Aldrich). The soybean oil was purified by gravity filtration through a column packed with a 1 : 1 mixture of fluorisil and silica gel (100–200 mesh, Sigma-Aldrich). This served to remove surface-active contaminants (*e.g.* monoglycerides), such that the equilibrium interfacial tension at the oil–water interface matched the reported value for purified soybean oil in the literature ( $\gamma = 31\ \text{mN m}^{-1}$ ).<sup>57</sup> We also measured the surface tension of the oil–water interface with 2 mM DOPC dissolved in the oil-phase:  $\gamma = 15.9 \pm 0.3\ \text{mN m}^{-1}$ .<sup>48</sup> These measurements indicate that the purified soybean oil contains negligible amphiphiles, such that the DOPC lipids are the dominant surfactant at the oil–water interface. 1,2-dioleoyl-*sn*-glycero-3-phosphocholine dissolved in chloroform (DOPC, Avanti Polar Lipids, 850375C) was dried under a gentle inert gas flow (1 h, room temperature) and further dried under vacuum (2 h, room temperature). The dried lipids were then dissolved in oil by shaking overnight (2 mM, 37 °C, 250 rpm). When using fluorescent imaging, 1,2-dipalmitoyl-*sn*-glycero-3-phosphoethanolamine-*N*-(lissamine rhodamine B sulfonyl) (ammonium salt) (DOPC, Avanti Polar Lipids, 810158C) (0.1 mol%) was added to the DOPC before dissolving in oil.

### 2.3. Preparation of lipid–water mixtures

The lipid–water mixture preparation method was similar to the lipid–oil mixture preparation, except for the following steps. The dried lipids were dissolved in deionized water instead of oil. To prepare unilamellar liposomal suspensions with a low polydispersity, the modified protocol from the Large, Unilamellar Vesicles by Extrusion (LUVET) technique (Avanti Polar Lipids) was used. The hydrated lipid suspension was subjected to 4 freeze/thaw cycles by alternately placing the mixture vial inside ( $-20\ ^\circ\text{C}$ ) and outside (room temperature) of a freezer to increase the entrapment efficiency of water-soluble compounds. Once the mixture was completely hydrated, it was then extruded with  $0.1\ \mu\text{m}$  pore size membranes to obtain the unilamellar liposomal suspensions. The lipid suspension was kept above the phase transition temperature of the lipid during hydration and extrusion.

### 2.4. $\mu$ DIB formation (in microfluidic device)

The lipid-in and lipid-out methods were alternatively used to form microscale droplet interface bilayers ( $\mu$ DIBs) by joining femtoliter-volume droplets submerged in oil under a constant temperature ( $25\ ^\circ\text{C}$ ). Using the previously described microfluidic device, the two side-channels were filled with water while the central channel was filled with oil. The water droplets were generated by an abrupt change in height from the side channels to the larger central channel, resulting in shape induced pinch-off upon application of timed pressure pulses to the opposing

side channels.<sup>57</sup> The droplets were then joined together in the central oil channel to form  $\mu$ DIBs upon contact. The microfluidic device facilitates the rapid assembly of the droplets with a well-defined time zero.<sup>59</sup> When using the lipid-out method, the lipids were dissolved in the central oil channel. For the lipid-in method, the lipids were in the water channels.

In both cases, after the lipid monolayer droplets were formed in the central oil channel, the central channel was pressurized to bring the droplets into a larger outlet reservoir. This served to minimize wetting and to prevent side-wall effects. Once the droplets had joined together to form a  $\mu$ DIB, the oil flow was stopped to observe the droplets evaporate over time. A CCD camera (CoolSNAP HQ from Roper Scientific and Evolve™ 512 Delta from Photometrics) connected to an inverted optical microscope (Eclipse TE 300, Nikon Instruments) with a 100 $\times$  oil-immersion objective was employed to acquire bright-field and fluorescent imaging. All experiments were performed in a microscope cage incubator (Okolab H201) to maintain a constant temperature of 25 °C.

### 2.5. $\mu$ DIB formation (on glass substrate)

In another approach, a system consisting of a commercially available microinjector (Femtojet, Eppendorf) and a motorized micromanipulator (SM325, World Precision Instruments, Inc.) was used to dispense microscale water droplets ( $D \approx 50 \mu\text{m}$ ) in a thin oil lens on a glass coverslip. The microinjector consists of a pressure pump that can apply a controlled pressure (0–600 kPa) on the fluid contained in a glass micropipette (Femtotip II, Eppendorf) with a tip diameter of 0.5  $\mu\text{m}$ . In this non-microfluidic approach,  $\mu$ DIBs were formed by the following procedure: 22 mm  $\times$  22 mm coverglasses (Fisher Scientific) were silanized using a standard silanizing procedure to prevent wetting. A 40  $\mu\text{L}$  oil lens containing 2 mg  $\text{mL}^{-1}$  ( $\approx 2.36 \text{ mM}$ ) DOPC was manually pipetted on the glass after mildly rinsing the silanized coverglass with DI water. The height of the oil lens on the glass was between 200 and 350  $\mu\text{m}$ . After pre-filling the glass pipette with deionized water, the tip of the pipette was positioned under the oil lens such that it touches the coverglass surface at an angle less than 45° to prevent damaging the tip. The position of the pipette tip was viewed using an inverted microscope (Olympus, IX51). Droplets were dispensed by gently dragging the pipette tip across the glass while applying a constant pressure using the microinjector; the dragging motion facilitates droplet breakoff and helps dictate the size of the dispensed aqueous droplet. Once the droplets were dispensed, they were connected to form  $\mu$ DIBs using the pipette tip. The measured droplet-shrinking rate (120–500  $\mu\text{m}^2 \text{ min}^{-1}$ ) depends on the volume of oil surrounding the droplets and is different from the rate measured in the microfluidic device.

## 3. Results and discussion

By using both the lipid-in and lipid-out methods to form  $\mu$ DIBs from femtoliter-volume water droplets, three different initial conditions were obtained for lipid distribution in the system: lipids dissolved evenly in the oil phase (lipid-out in soybean oil),

vesicles inside of the water droplets (lipid-in), and lipid agglomerates in the oil (lipid-out in hexadecane). The lipid used for all experiments was 1,2-dioleoyl-*sn*-glycero-3-phosphocholine (DOPC, Avanti Polar Lipids, 850375C), selected for its low transition temperature of  $-20 \text{ }^\circ\text{C}$  to ensure that the lipids are in the liquid phase at room temperature. Experiments carried out in dry poly(dimethylsiloxane) (PDMS) microfluidic device resulted in a shrinkage rate of  $\sim 100 \mu\text{m}^2 \text{ min}^{-1}$  for pure water droplets,<sup>60</sup> resulting in  $\mu$ DIB lifetimes of only 3–5 min for droplets with initial diameters of 5–10  $\mu\text{m}$  due to their large surface area to volume ratio ( $\sim 1 \mu\text{m}^{-1}$ ). Droplet shrinkage was driven by the osmotic pressure difference in the dry PDMS device, such that water molecules partitioned into the oil phase and pervaporated through the permeable PDMS walls.<sup>60</sup> For simplicity, we will use the term evaporation when describing this process of droplet shrinkage. As the droplets evaporated, the dynamics of lipid transfer between the membrane interfaces was observed and characterized into three different classes depending on the initial conditions, as described below.

### 3.1. Class 1: buckling and fission

The lipid-out method, with DOPC dissolved in purified soybean oil, was used to form  $\mu$ DIBs (Fig. 1). Due to the energetic favorability of the formed bilayer, the bilayer did not shrink during evaporation. The preferential shrinkage of the monolayer interfaces resulted in a “conveyor-belt” effect during droplet evaporation, where lipids in the shrinking monolayers continually paired together and transferred into the growing bilayer to conserve their mass.

A non-dimensional parameter,  $A^*$ , can be used to compare the surface areas of the lipid monolayers *versus* the lipid bilayer over time,

$$A^* \sim \frac{2A_b}{A_{m-r} + A_{m-l}} \quad (1)$$

where  $A_b$ ,  $A_{m-r}$ , and  $A_{m-l}$  are the measured interfacial areas of the bilayer, right droplet monolayer, and left droplet monolayer, respectively. The areas were extrapolated from measurements of the bilayer diameter and droplet diameters when focusing on the maximal cross-section of the droplets. The transfer of lipids from the monolayers to the bilayer is quantitatively depicted in Fig. 2, where  $A^*$  continuously increased from  $A^* \approx 0.3$  to  $A^* \approx 0.5$  during evaporation. The continued growth of the bilayer resulted in three distinct regimes during evaporation which are outlined below.

**3.1.1. Regime 1: shape-change.** As both droplets evaporated, the monolayer interfaces changed shape to assume the most energetically favorable configuration: a single spherical droplet partitioned into two hemi-spheres by the lipid bilayer (Fig. 1). The bilayer interfacial area did not remain constant during evaporation, but actually increased from  $A_b \approx 42 \mu\text{m}^2$  to  $A_b \approx 57 \mu\text{m}^2$  as the droplets evaporated and changed shape (Fig. 2). Bilayer growth was fuelled by the shrinkage of the monolayer interfaces, which forced lipids in the monolayers to pair together and slide into the bilayer. The average surface area lost by the monolayers during the shape-change was

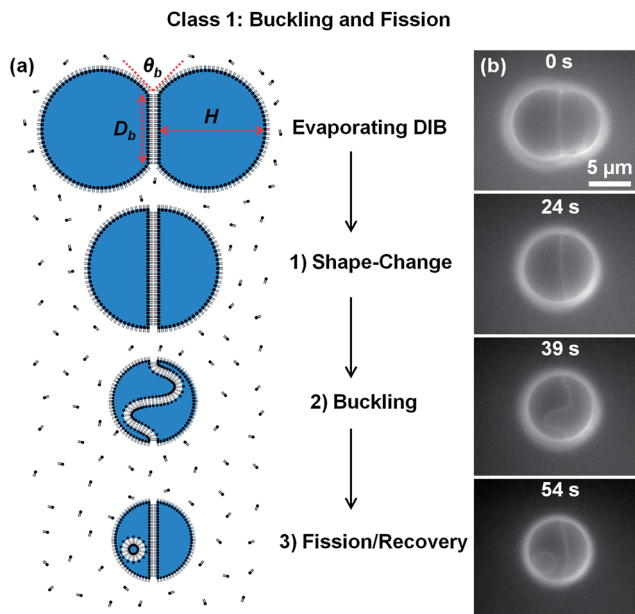


Fig. 1 (a) Schematic and (b) fluorescent imaging of an evaporating μDIB experiencing buckling and fission (Section 3.1). The lipid-out technique was used to dissolve DOPC lipids in soybean oil. During droplet evaporation, lipids transferred from the monolayers to the bilayer, resulting in bilayer confinement, buckling, and fission. See Movie M1 in ESI.†

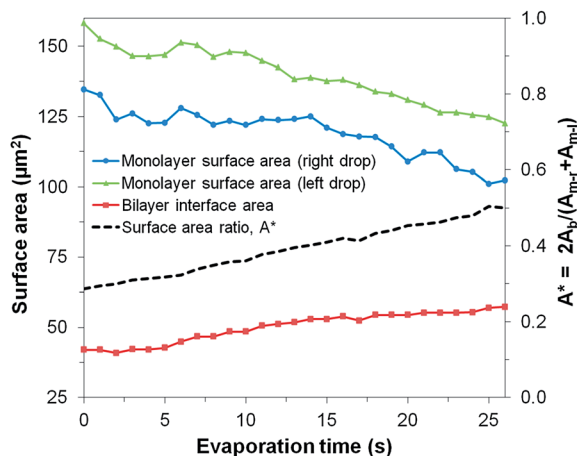


Fig. 2 Evolution of the surface areas of the monolayers and bilayer for an evaporating μDIB system experiencing buckling and fission (corresponding to Fig. 1b). The ratio of bilayer area to monolayer area ( $A^*$ ) steadily increases during evaporation, resulting in bilayer buckling.

approximately 34 μm<sup>2</sup> each, about twice as large as the interfacial area gained by the bilayer (~15 μm<sup>2</sup>) (Fig. 2). This imperfect conservation of mass suggests either an increase in the packing density of the lipids, desorption of some monolayer lipids back into the oil,<sup>55</sup> or the formation of nanoscale protuberances which could not be optically resolved.<sup>17,61</sup> It is currently unclear whether the monolayer or bilayer surface tensions are changing during evaporation; in the future, it is possible that a microtensiometer apparatus could probe the dynamic changes in membrane surface tensions.<sup>55,62</sup>

In addition to forming a single μDIB between a pair of droplets, multiple μDIBs were formed using a 3-droplet cluster configuration, a 5-droplet cluster, or a 10-droplet chain. For the 3-droplet cluster, the system still evaporated into the shape of a single sphere, but now the interior was partitioned into three equivalent compartments by three bilayers (Fig. 3a). Similarly, the 5-droplet cluster evaporated into a sphere with five compartments (Fig. 3b). In contrast, the droplets in the chain configuration could not morph into a single spherical shape because of the intermediate bilayers, which would have to be ruptured to bring all of the droplets together. Therefore, the droplets preferred to longitudinally shrink from both ends toward the center of the chain (Fig. 3c).

**3.1.2. Regime 2: bilayer buckling.** Once the droplets evolved into the shape of a single spherical droplet, the system retained this spherical configuration for the duration of evaporation. This is due to the spherical shape corresponding to the energetic minimum of the system.<sup>48</sup> The fixed spherical shape causes the encapsulated bilayer to become confined as it continues to grow inside of the shrinking sphere. Because the lipid bilayer is relatively incompressible compared to its low bending stiffness,<sup>63,64</sup> the confined bilayer is forced to buckle with an increasingly curved shape as it continues to grow (Fig. 1b). Area measurements in Fig. 2 were only obtained for the shape-change regime, as the curvature of the

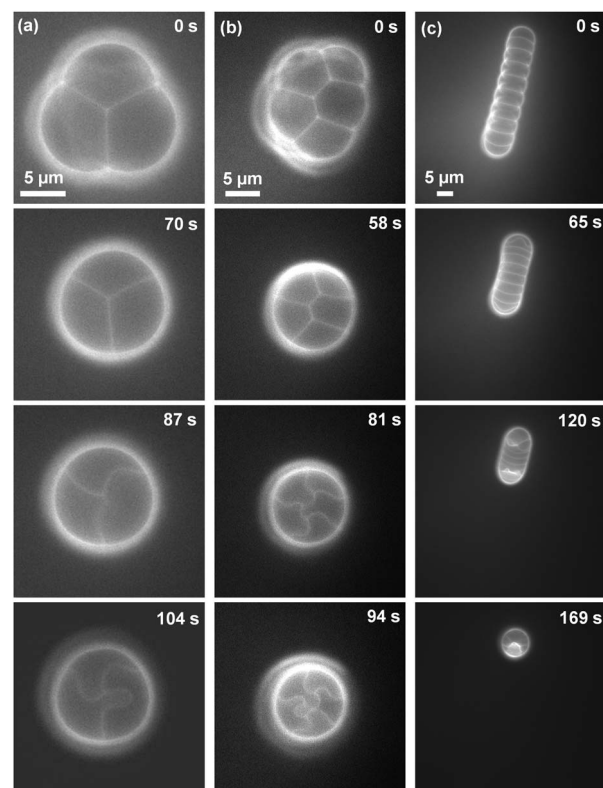


Fig. 3 Fluorescent imaging of evaporating μDIB networks experiencing buckling: (a) 3-droplet cluster, (b) 5-droplet cluster and (c) 10-droplet chain. Aside from the increased number of water droplets brought together, the experimental conditions were identical to those used in Fig. 1b. See Movies M2–M4 in ESI.†

buckling bilayer makes it difficult to accurately estimate its surface area.

For the 3-droplet and 5-droplet clusters, all bilayers buckled in tandem as they became confined inside of the sphere (Fig. 3a). In contrast, the bilayers in the chain network preferentially grew and buckled at the ends of the chain (Fig. 3c). This is due to the interfacial area of the monolayers being greater at the ends of the chain, resulting in enhanced evaporation and shape-change compared to the middle of the chain. As evaporation continued, lipid bilayers in the middle of the chain also became confined, buckling in a chain reaction that propagated from the ends of the chain.

**3.1.3. Regime 3: fission/recovery.** The confined bilayer became increasingly buckled until reaching a critical radius of curvature, at which point the bilayer fissioned a lipid vesicle approximately 2  $\mu\text{m}$  in diameter into one of the hemi-spherical droplets (Fig. 1b). This loss of lipid mass restored the bilayer to a more planar configuration, thereby mitigating its bending stress. As the  $\mu\text{DIB}$  system continued to shrink, the bilayer became buckled again, cycling through the buckling and fission/recovery regimes until all water content in the droplets had evaporated (see Movie M1 in ESI†). It was observed that when droplets had different sizes, the shape-change during evaporation was asymmetric, causing the bilayer to preferentially buckle and fission toward the compartment corresponding to the larger droplet (Fig. 1b). This directional buckling and fission is caused by the differing radii of curvature between droplets of different sizes, which creates a greater Laplace pressure in the smaller droplet.

For droplet clusters and chains, fission could not be observed due to the buckling bilayers contacting adjacent monolayers and/or bilayers before reaching the critical radius of curvature (Fig. 3). However, this scenario apparently serves as an alternative strategy for mitigating bilayer stress. As the buckling bilayer contacts another interface, budding occurs, which creates new interfacial area to manage stress.

### 3.2. Class 2: uniform shrinking

When forming DIBs with the lipid-in method, the lipids are dispersed in the aqueous phase instead of in the oil phase.<sup>23</sup> Here, DOPC lipids were mixed in the water to create  $\mu\text{DIBs}$ . Hexadecane was used as the continuous oil phase, as it was observed that soybean oil often resulted in droplet coalescence instead of  $\mu\text{DIB}$  formation when using the lipid-in method. The lipid-in method results in lipid vesicles distributed within the water droplets, which can be observed by fluorescently labelling the lipids (Fig. 4b). Unlike the “buckling and fission” class, where loss of monolayer interfacial area was compensated by a growing bilayer area, all interfaces were observed to shrink over time (Fig. 4). During evaporation, the monolayer interfaces shrunk at an equivalent rate of  $\dot{A}_{m-l} \approx \dot{A}_{m-r} \approx -1.1 \mu\text{m}^2 \text{s}^{-1}$ , while the droplet interface bilayer decreased by  $\dot{A}_b \approx -0.23 \mu\text{m}^2 \text{s}^{-1}$  (Fig. 5). The ratio of bilayer area to monolayer area ( $A^*$ , see eqn (1)) remained constant throughout the lifetime of the droplets (Fig. 5), preserving the original shape of the droplets (Fig. 5), preserving the original shape of the droplets. Both droplets continued to shrink uniformly until all of the water had

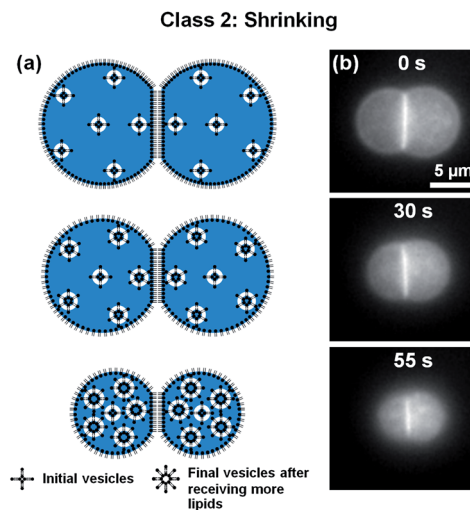


Fig. 4 (a) Schematic and (b) fluorescent imaging of an evaporating  $\mu\text{DIB}$  experiencing uniform shrinkage (Section 3.2). The lipid-in technique was employed, such that the water droplets contained vesicles of DOPC lipids. During evaporation, lipids transferred from the monolayers and bilayer to the vesicles, resulting in the uniform shrinkage of the droplets. See Movie M5 in ESI.†

evaporated, without any indication of shape-change, buckling, or fission (Fig. 4). A 5-droplet cluster of droplets was also observed to shrink uniformly during evaporation (Fig. 6).

Considering the favorable hydrophobic interactions between the tail groups of a lipid bilayer, the observed shrinkage of the bilayer over time is somewhat surprising. One possible explanation for the shrinking bilayer is surface tension. The equilibrium contact angle of a droplet interface bilayer ( $\theta_b$ ) is governed by a balance of the surface tension vectors at the droplet–droplet contact line:<sup>39</sup>

$$2\gamma_m \cos\left(\frac{\theta_b}{2}\right) = \gamma_b \quad (2)$$

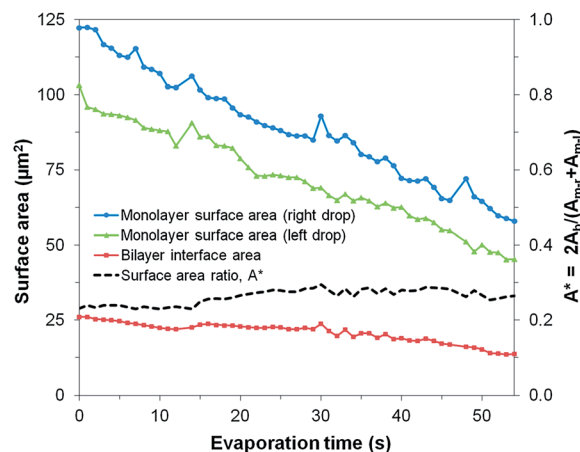


Fig. 5 Evolution of the surface areas of the monolayers and bilayer for a uniformly shrinking  $\mu\text{DIB}$  system (corresponding to Fig. 4b). The ratio of bilayer area to monolayer area ( $A^*$ ) was constant throughout evaporation, preserving the system's shape and equilibrium contact angle.

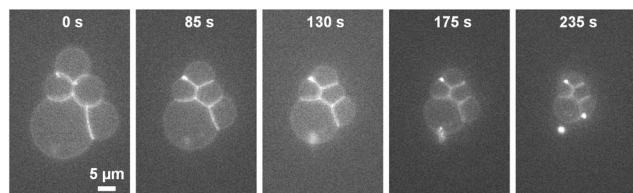


Fig. 6 Using the lipid-in technique, a 5-droplet cluster exhibited uniform shrinking similar to the 2-droplet example (Fig. 4b). This indicates that  $\mu$ DIBs systems containing vesicles in the water droplets are able to shrink uniformly regardless of their initial shape. See Movie M6 in ESI.†

where  $\gamma_m$  and  $\gamma_b$  correspond to the surface tensions of the monolayers and bilayer, respectively.

The contact angle is related to the bilayer diameter ( $D_b$ ) and droplet height ( $H$ ) by  $\theta_b = 2\pi - 4 \tan^{-1}(2H/D_b)$ , where  $H$  extends from the bilayer to the opposing monolayer interface (Fig. 1a). In other words, the ratio  $2H/D_b$  must remain constant over time to maintain the value of  $\theta_b$  corresponding to equilibrium. A constant ratio of  $2H/D_b \approx 1.8 \pm 0.2$  is measured throughout droplet evaporation, with the uncertainty corresponding to a 95% confidence interval. This proportional shrinkage of the monolayer and bilayer interfaces indicates that the surface tension vectors at the contact line remain balanced throughout evaporation.

The lipid-in approach to forming  $\mu$ DIBs enables lipids to transfer from both the monolayers and the bilayer to adjacent vesicles located inside of the water droplets. Since the vesicles are always hydrated by a surrounding water droplet, they can accommodate additional lipids without becoming stressed. In contrast to lipid-out  $\mu$ DIBs, where the bilayer managed its stress *via* buckling and fission, lipid-in  $\mu$ DIBs seem to manage their stress *via* lipid transfer to vesicles to completely avoid buckling or fission events.

### 3.3. Class 3: stretching and unzipping

When the lipid-out method was employed to generate  $\mu$ DIBs in a DOPC/hexadecane bath, microscale clusters of lipid agglomerates were observed throughout the hexadecane.<sup>65</sup> This was in contrast to using the lipid-out method with soybean oil, where the lipids dissolved more evenly in the oil (Section 3.1). The presence of these lipid agglomerates affected the wettability and dynamic morphology of the  $\mu$ DIB system during evaporation.

During evaporation, the right droplet's monolayer interface was observed to shrink at a rate of approximately  $\dot{A}_{m-r} \approx -3.3 \mu\text{m}^2 \text{s}^{-1}$ , faster than the  $\dot{A}_{m-l} \approx -2.6 \mu\text{m}^2 \text{s}^{-1}$  evaporation rate of the left droplet. The accelerated evaporation of the right droplet was correlated with a higher concentration of lipid agglomerates that visibly clustered around the right droplet (Fig. 7). Over multiple trials, it was consistently observed that droplet shrinkage was always accelerated wherever agglomerates were most concentrated at a droplet interface. In some cases, the evaporation rate of one droplet could be over three times faster than its partner due to the inhomogeneous distribution of lipid agglomerates (Fig. S1†). Even for the case of two isolated

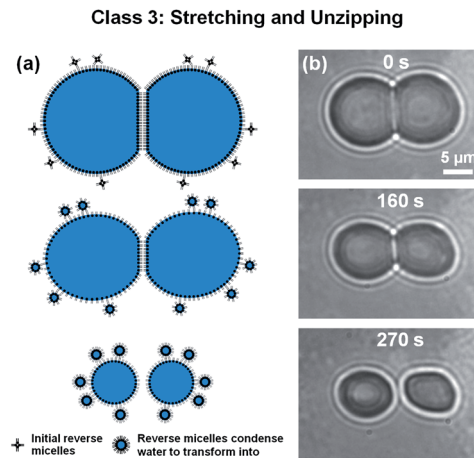


Fig. 7 (a) Schematic and (b) bright-field imaging of a  $\mu$ DIB exhibiting stretching and unzipping during evaporation (Section 3.3). Using the lipid-out approach with DOPC and hexadecane, microscale agglomerates of lipids were visible in the oil. These agglomerates caused droplet pinning at a PDMS wall, resulting in the stretching and separation of the droplets. During evaporation, the water droplets hydrated adjacent lipid agglomerates, and lipids were transferred from the parent droplets to the condensing satellite droplets. See Movie M7 in ESI.†

droplets, where no bilayer was present, the droplet that was adjacent to a cluster of agglomerates was observed to evaporate four times faster than a nearby droplet that was not in contact with any agglomerates (Fig. S2†). Therefore, it can be concluded that the lipid agglomerates serve to locally accelerate the rate of water evaporation. This is most likely due to the reverse micellar configuration of lipids in oil, which thermodynamically favor the condensation of water at the center of the reverse micelle where the hydrophilic heads groups congregate.

The average area loss in the monolayers was  $\approx 160 \mu\text{m}^2$  ( $\approx 141 \mu\text{m}^2$  for the left droplet and  $\approx 180 \mu\text{m}^2$  for the right droplet) and the area lost from the bilayer was  $\approx 85 \mu\text{m}^2$  (Fig. 8). Assuming that the lipid concentration at the interfaces was initially close to equilibrium, the shrinkage of every lipid interface in the  $\mu$ DIB system mandates the desorption/transfer of some of the lipids away from the droplets.<sup>55</sup> From the observation that the agglomerates of reverse micelles serve to enhance the evaporation rate of the droplets, it can be assumed that the reverse micelles are becoming hydrated by the droplets over time. The hydration of a reverse micelle would swell its interface to accommodate lipid transfer from the shrinking monolayer interfaces of the  $\mu$ DIB system. In other words, the shrinkage of the original droplet interfaces is balanced by the nucleation and growth of satellite droplets, with lipids transferring from the former to the latter to conserve their mass (as illustrated in Fig. 7a).

The unzipping of the bilayer was completed well before the droplets finished evaporating ( $A^* \rightarrow 0$ ), resulting in the complete separation of the droplets (Fig. 8). This is in contrast to the “uniform shrinking” class (Section 3.2), where the shrinkage rate of the bilayer was proportional to that of the monolayers (constant  $A^*$ ). The complete unzipping of the

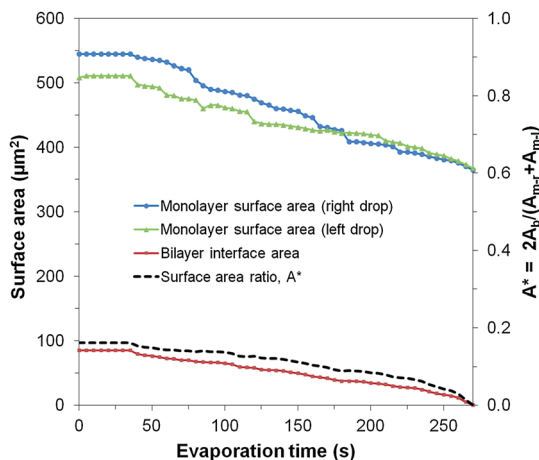


Fig. 8 Evolution of the surface areas of the monolayers and bilayer for an evaporating  $\mu$ DIB system experiencing stretching and unzipping (corresponding to Fig. 7b). The preferential unzipping of the bilayer is represented by the surface area ratio  $A^*$  decreasing to zero.

bilayer was attributed to wettability effects, as the droplets were observed to pin onto agglomerates that were stuck to a wall of the PDMS channel. As the droplets evaporated, pinning effects prevented them from freely reconfiguring their center of mass, such that they eventually became stretched and pulled the bilayer apart. The strong pinning of a droplet due to adjacent agglomerates was well evidenced by the droplet's increasingly non-circular footprint during evaporation. Even after separation, the contact line of a pinned droplet was non-circular, and the remaining water volume was rapidly collected by the adjacent lipid agglomerates. This behavior was also observed for chains and clusters of pinned droplets, where droplets closest to the agglomerates were the first to stretch and unzip from the group of droplets (Fig. S3<sup>†</sup>).

Unlike the DOPC/hexadecane mixture, where microscale clusters of lipid agglomerates formed in the oil phase and facilitated the pinning of droplets onto a channel wall, the DOPC/soybean oil mixture had no visible lipid agglomerates. Even when water droplets immersed in soybean oil were visibly wetting a wall of the channel, the droplets' contact lines were able to recede along the wall during evaporation to prevent any stretching or unzipping (Fig. S4<sup>†</sup>). Therefore, it is likely that the agglomerates present in the hexadecane serve to enhance droplet wettability on a wall(s), resulting in the strong pinning of the droplet's contact line. This indicates that wetting alone is not a sufficient condition for stretching and unzipping to occur; the wetted contact line must be pinned to the surface.

To determine whether the large (microscale) agglomerates of lipids visible in the hexadecane were necessary for the satellite droplets to form, another batch of DOPC/hexadecane was mixed, this time with no visible agglomerates. To enhance the optical characterization of the  $\mu$ DIB system, a microinjector was used to deposit water droplets inside of an oil lens instead of using the microfluidic device. The oil lens was resting on a silanized glass substrate to facilitate bottom-up microscopy, and the droplet diameter was increased by an order of

magnitude compared to the microfluidic droplets ( $\approx 50 \mu\text{m}$  instead of  $\approx 5 \mu\text{m}$ ) to improve the image quality. At time zero, the  $\mu$ DIB system was free of any visible lipid agglomerates or satellite droplets. However, as the droplets evaporated, hundreds of satellite droplets nucleated and grew at the monolayer interface of both droplets (Fig. 9). This confirms that water droplets serve to hydrate reverse micelles located nearby in the oil phase, even when the reverse micelles are well distributed and too small to be visible. The initial nucleation of a satellite droplet serves to hydrate the hydrophilic head groups of lipids in a reverse micelle, while the subsequent growth of the satellite droplet serves to accommodate additional lipids from the evaporating parent droplet.

While the presence of a bilayer between a satellite droplet and the parent droplet could not be visually resolved, it seems more likely than the alternate possibility of budding for the following reasons:

(1) The growth of the satellite droplets corresponds to an accelerated evaporation rate for the parent droplet (see Fig. S2<sup>†</sup>). Budding effects would be independent of such phase-change behavior, but satellite droplets would indeed require water vapor to partition from the parent droplet into the oil phase.

(2) Unlike bilayer budding that can occur on the surface of a vesicle/cell, the surfaces of our droplets are composed of lipid monolayers. While lipid monolayers can collapse due to compression (loss of tension) at both air–water interfaces<sup>66,67</sup> and oil–water interfaces,<sup>68</sup> the collapsing lipid monolayers eject lipids into the polar aqueous phase rather than the non-polar phase. Thus, we'd expect collapsing lipid monolayers during droplet shrinkage to eject lipid material back into the droplet interior instead of the surrounding oil.

(3) Satellite droplets exhibit a strong resistance to coalescence, merging together only after very tight packing (see Fig. 9). This aversion to coalescence would not be expected for budding, as adjacent buds would minimize their surface energy by merging together. Satellite droplets, on the other hand, would require the disruption of their separate bilayers which could provide an energy barrier to merging.

To our knowledge, the nucleation of satellite droplets about the interface of a water droplet evaporating in a lipid–oil bath is

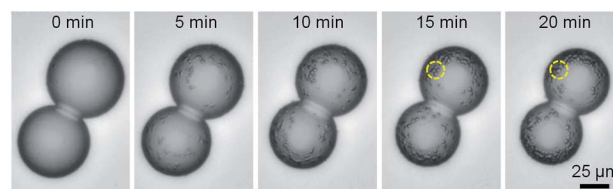


Fig. 9 Bright-field imaging of a  $\mu$ DIB system condensing satellite droplets about the droplet interfaces. Reverse micelles in the oil nucleate water to hydrate their hydrophilic head groups, and these satellite droplets grow over time to accommodate lipids from the shrinking parent droplet. Each satellite droplet forms a tiny  $\mu$ DIB with its parent droplet; these satellite droplets are free to migrate about the parent droplet's interface. Multiple satellite droplets can even coalesce together, as indicated by the yellow circle. See Movie M13 in ESI.<sup>†</sup>

a novel phenomenon that merits a brief discussion. While previous reports have characterized water confined inside of DOPC reverse micelles,<sup>69,70</sup> the hydration was caused by pre-existing water emulsions mixed uniformly into the oil, rather than by condensation from a nearby water droplet. For the results observed in Fig. 9, it should be noted that each satellite droplet is actually forming a new  $\mu$ DIB with its parent droplet, since both the original droplet and the satellite droplets exhibit lipid monolayers at their interfaces. This reveals that water evaporation and condensation can be a passive technique for generating both hydrated reverse micelles and droplet interface bilayers.

## 4. Conclusion

In conclusion, the dynamic morphology of evaporating  $\mu$ DIBs is dependent upon the initial distribution of lipids in the system and the wettability of the droplets. In the absence of lipid agglomerates or droplet pinning, lipids transfer from the monolayers to the bilayer during evaporation, culminating in the buckling and fission of the bilayer to mitigate its stress. When lipid vesicles are contained inside the water droplets, the monolayers and bilayer shrink uniformly to preserve the equilibrium contact angle of the system. When the droplets are pinned to a solid interface, the droplets become stretched and the bilayer breaks apart, resulting in the complete separation of the droplets. Evaporating water droplets can also generate entirely new  $\mu$ DIBs by hydrating reverse micelles to transform them into satellite droplets. This work reveals that the dynamic behavior of lipid interfaces can be widely varied by tuning the initial conditions of the system. Droplet interface bilayers show great potential as a tool for characterizing lipid transfer between interfaces, which could lead to a better understanding of natural phenomena such as endo- and exocytosis in cells.

## Acknowledgements

This research was conducted at the Center for Nanophase Materials Sciences, which is sponsored at Oak Ridge National Laboratory by the Scientific User Facilities Division, Office of Basic Energy Sciences, U.S. Department of Energy. G. Venkatesan and A. Sarles are funded by the Air Force Office of Scientific Research Basic Research Initiative grant number 11157642.

## Notes and references

- 1 J. E. Rothman, *Nature*, 1994, **372**, 55.
- 2 P. Walde, K. Cosentino, H. Engel and P. Stano, *ChemBioChem*, 2010, **11**, 848.
- 3 P. Mueller, D. O. Rudin, H. T. Tien and W. C. Wescott, *Nature*, 1962, **194**, 979.
- 4 M. Montal and P. Mueller, *Proc. Natl. Acad. Sci. U. S. A.*, 1972, **69**, 3561.
- 5 H. G. Dobereiner, J. Kas, D. Noppl, I. Sprenger and E. Sackmann, *Biophys. J.*, 1993, **65**, 1396.
- 6 W. Rawicz, B. A. Smith, T. J. McIntosh, S. A. Simon and E. Evans, *Biophys. J.*, 2008, **94**, 4725.
- 7 U. Seifert, K. Berndl and R. Lipowsky, *Phys. Rev. A: At., Mol., Opt. Phys.*, 1991, **44**, 1182.
- 8 F. M. Menger and S. J. Lee, *Langmuir*, 1995, **11**, 3685.
- 9 G. Staneva, M. I. Angelova and K. Koumanov, *Chem. Phys. Lipids*, 2004, **129**, 53.
- 10 T. Tanaka, R. Sano, Y. Yamashita and M. Yamazaki, *Langmuir*, 2004, **20**, 9526.
- 11 H. T. McMahon and J. L. Gallop, *Nature*, 2005, **438**, 590.
- 12 H. J. Woo and A. Wallqvist, *J. Phys. Chem. B*, 2011, **115**, 8122.
- 13 M. Andes-Koback and C. D. Keating, *J. Am. Chem. Soc.*, 2011, **133**, 9545.
- 14 Y. Li, H. Kusumaatmaja, R. Lipowsky and R. Dimova, *J. Phys. Chem. B*, 2012, **116**, 1819.
- 15 F. Julicher and R. Lipowsky, *Phys. Rev. E: Stat. Phys., Plasmas, Fluids, Relat. Interdiscip. Top.*, 1996, **53**, 2670.
- 16 M. Staykova, D. P. Holmes, C. Read and H. A. Stone, *Proc. Natl. Acad. Sci. U. S. A.*, 2011, **108**, 9084.
- 17 M. Staykova, M. Arroyo, M. Rahimi and H. A. Stone, *Phys. Rev. Lett.*, 2013, **110**, 028101.
- 18 Y. A. Domanov and P. K. J. Kinnunen, *Biophys. J.*, 2006, **91**, 4427.
- 19 D. Thid, J. J. Benkoski, S. Svedhem, B. Kasemo and J. Gold, *Langmuir*, 2007, **23**, 5878.
- 20 K. Giger, E. R. Lamberson and J. S. Hovis, *Langmuir*, 2009, **25**, 71.
- 21 K. Funakoshi, H. Suzuki and S. Takeuchi, *J. Am. Chem. Soc.*, 2007, **129**, 12608.
- 22 K. Funakoshi, H. Suzuki and S. Takeuchi, *Anal. Chem.*, 2006, **78**, 8169.
- 23 W. L. Hwang, M. Chen, B. Cronin, M. A. Holden and H. Bayley, *J. Am. Chem. Soc.*, 2008, **130**, 5878.
- 24 R. Syeda, M. A. Holden, W. L. Hwang and H. Bayley, *J. Am. Chem. Soc.*, 2008, **130**, 15543.
- 25 S. A. Sarles and D. J. Leo, *Lab Chip*, 2010, **10**, 710.
- 26 S. Punnamaraju and A. J. Steckl, *Langmuir*, 2011, **27**, 618.
- 27 A. Fischer, M. A. Holden, B. L. Pentelute and R. J. Collier, *Proc. Natl. Acad. Sci. U. S. A.*, 2011, **108**, 16577.
- 28 S. A. Sarles, *Smart Mater. Struct.*, 2013, **22**, 094023.
- 29 M. A. Holden, D. Needham and H. Bayley, *J. Am. Chem. Soc.*, 2007, **129**, 8650.
- 30 W. L. Hwang, M. A. Holden, S. White and H. Bayley, *J. Am. Chem. Soc.*, 2007, **129**, 11854.
- 31 Y. Tsuji, R. Kawano, T. Osaki, K. Kamiya, N. Miki and S. Takeuchi, *Lab Chip*, 2013, **13**, 1476.
- 32 M. Yanagisawa, T. Yoshida, M. Furuta, S. Nakata and M. Tokita, *Soft Matter*, 2013, **9**, 5891.
- 33 G. Maglia, A. J. Heron, W. L. Hwang, M. A. Holden, E. Mikhailova, Q. Li, S. Cheley and H. Bayley, *Nat. Nanotechnol.*, 2009, **4**, 437.
- 34 S. Punnamaraju, H. You and A. J. Steckl, *Langmuir*, 2012, **28**, 7657.
- 35 S. A. Sarles and D. J. Leo, *J. Intell. Mater. Syst. Struct.*, 2009, **20**, 1233.
- 36 M. Lein, J. Huang and M. A. Holden, *Lab Chip*, 2013, **13**, 2749.

- 37 S. Leptihn, O. K. Castell, B. Cronin, E. Lee, L. C. M. Gross, D. P. Marshall, J. R. Thompson, M. Holden and M. I. Wallace, *Nat. Protoc.*, 2013, **8**, 1048.
- 38 S. S. Dixit, H. Kim, A. Vasilyev, A. Eid and G. W. Faris, *Langmuir*, 2010, **26**, 6193.
- 39 S. S. Dixit, A. Pincus, B. Guo and G. W. Faris, *Langmuir*, 2012, **28**, 7442.
- 40 S. A. Sarles and D. J. Leo, *Anal. Chem.*, 2010, **82**, 959.
- 41 S. Aghdaei, M. E. Sandison, M. Zagnoni, N. G. Green and H. Morgan, *Lab Chip*, 2008, **8**, 1617.
- 42 J. L. Poulos, W. C. Nelson, T. J. Jeon, C. J. Kim and J. J. Schmidt, *Appl. Phys. Lett.*, 2009, **95**, 013706.
- 43 A. Martel and B. Cross, *Biomicrofluidics*, 2012, **6**, 012813.
- 44 C. E. Stanley, K. S. Elvira, X. Z. Niu, A. D. Gee, O. Ces, J. B. Edel and A. J. deMello, *Chem. Commun.*, 2010, **46**, 1620.
- 45 Y. Elani, A. J. deMello, X. Niu and O. Ces, *Lab Chip*, 2012, **12**, 3514.
- 46 A. R. Thiam, N. Bremond and J. Bibette, *Langmuir*, 2012, **28**, 6291.
- 47 G. Villar, A. D. Graham and H. Bayley, *Science*, 2013, **340**, 48.
- 48 J. B. Boreyko, P. Mruetusatorn, S. A. Sarles, S. T. Retterer and C. P. Collier, *J. Am. Chem. Soc.*, 2013, **135**, 5545.
- 49 I. Reviakine and A. Brisson, *Langmuir*, 2000, **16**, 1806.
- 50 J. M. Johnson, T. Ha, S. Chu and S. G. Boxer, *Biophys. J.*, 2002, **83**, 3371.
- 51 E. Reimhult, F. Hook and B. Kasemo, *Langmuir*, 2003, **19**, 1681.
- 52 R. P. Richter, R. Berat and A. R. Brisson, *Langmuir*, 2006, **22**, 3497.
- 53 N. Hain, M. Gallego and I. Reviakine, *Langmuir*, 2013, **29**, 2282.
- 54 P. Plunkett, B. A. Camley, K. L. Weirich, J. Israelachvili and P. J. Atzberger, *Soft Matter*, 2013, **9**, 8420.
- 55 N. J. Alvarez, L. M. Walker and S. L. Anna, *Langmuir*, 2010, **26**, 13310.
- 56 S. Thutupalli, J. B. Fleury, A. Steinberger, S. Herminghaus and R. Seemann, *Chem. Commun.*, 2013, **49**, 1443.
- 57 S. Y. Jung, S. T. Retterer and C. P. Collier, *Lab Chip*, 2010, **10**, 2688.
- 58 S. Y. Jung, S. T. Retterer and C. P. Collier, *Lab Chip*, 2010, **10**, 3373.
- 59 S. Y. Jung, Y. Liu and C. P. Collier, *Langmuir*, 2008, **24**, 4439.
- 60 J. B. Boreyko, P. Mruetusatorn, S. T. Retterer and C. P. Collier, *Lab Chip*, 2013, **13**, 1295.
- 61 Y. Li, R. Lipowsky and R. Dimova, *Proc. Natl. Acad. Sci. U. S. A.*, 2011, **108**, 4731.
- 62 N. Anton, P. Pierrat, L. Lebeau, T. F. Vandamme and P. Bouriat, *Soft Matter*, 2013, **9**, 10081.
- 63 E. Sackmann, *FEBS Lett.*, 1994, **346**, 3.
- 64 L. J. Lis, M. McAlister, N. Fuller, R. P. Rand and V. A. Parsegian, *Biophys. J.*, 1982, **37**, 667.
- 65 R. Gupta, H. S. Muralidhara and H. T. Davis, *Langmuir*, 2001, **17**, 5176.
- 66 S. Baoukina, L. Monticelli, M. Amrein and D. P. Tieleman, *Biophys. J.*, 2007, **93**, 3775.
- 67 S. Baoukina, L. Monticelli, H. J. Risselada, S. J. Marrink and D. P. Tieleman, *Proc. Natl. Acad. Sci. U. S. A.*, 2008, **105**, 10803.
- 68 W. X. Shi and H. X. Guo, *J. Phys. Chem. B*, 2010, **114**, 6365.
- 69 N. E. Levinger, R. Costard, E. T. J. Nibbering and T. Elsaesser, *J. Phys. Chem. A*, 2011, **115**, 11952.
- 70 R. Costard, N. E. Levinger, E. T. J. Nibbering and T. Elsaesser, *J. Phys. Chem. B*, 2012, **116**, 5752.